**Modeling of Casting, Welding, and Advanced Solidification Processes - XII**
*Edited by: Steve L. Cockcroft and Daan M. Maijer*
***TMS (The Minerals, Metals & Materials Society), 2009***

# USING A FIVE-PHASE VOLUME AVERAGING APPROACH TO MODEL THE MIXED COLUMNAR-EQUIAXED SOLIDIFICATION

M. Wu and A. Ludwig

Simulation and Modeling of Metallurgical Processes, Dept. of Metallurgy
University of Leoben, A-8700, Austria

Keywords: dendritic growth, mixed columnar-equiaxed solidification, columnar-to-equiaxed transition, melt convection, grain sedimentation, macrosegregation

## Abstract

A previous mixed columnar-equiaxed solidification model, developed by the current authors, is extended to include the dendritic morphology. Five phase regions (phases) must be considered: the interdendritic melt and solid dendrites in equiaxed grains, the interdendritic melt and solid dendrites in columnar dendrite trunks, the extra melt. The five phase regions are quantified by their volume fractions, and characterized by different solute concentrations. They are transported with the velocities of the so-called 'hydrodynamic' phases. Here three 'hydrodynamic' phases are distinguished: the extra melt, the equiaxed grains combining the interdendritic melt and solid dendrites, and the columnar trunks combining the interdendritic melt and solid dendrites. The shape of the grain/trunk envelopes, separating the extra melt from the interdendritic melts, are described with the morphological parameters. Evolutions of the envelopes are derived from the growth kinetics: Kurz-Giovanola-Trivedi model for the columnar primary dendrite tips, Lipton-Glicksman-Kurz model for the columnar trunks (radial direction) and the equiaxed dendrites. The solidification of the interdendritic melt is governed by the diffusion in the interdendritic melt region.

## Introduction

Wang and Beckermann [1-2] have outlined a general multiphase approach to deal with the dendritic morphology in equiaxed or columnar solidification. With the idea similar to the Rappaz and Thevoz' model [3-4], a grain envelope is defined to separate the extra melt from the interdendritic melt. Because columnar dendrite trunks and equiaxed grains have different morphologies, different formulations and morphological parameters must be considered. The current work is to extend a previous 3-phase mixed columnar-equiaxed solidification model of the authors [5-6] by including the dendritic morphologies. The main features of the previous 3-phase mixed columnar-equiaxed solidification model is to consider melt convection, grain sedimentation, columnar tip front tracking, interaction between equiaxed grains and columnar dendrite trunks, columnar-to-equiaxed transition, etc. The current paper will give a general description of model. It includes the phase definition, the treatment of the equiaxed and columnar dendrite morphologies and the growth kinetics. Demonstrative modelling results based on an Al-Cu cylindrical casting will be presented: the evolution and transport of the phases, formation of the equiaxed zone and mixed columnar-equiaxed zone separated by CET, interdendritic and extra grain eutectics, and the formation of the macrosegregation.

## Model

*Phase definition*

As shown in Fig. 1, 5 phase regions are distinguished: extra melt, interdendritic melt in the equiaxed grain, solid dendrites in the equiaxed grain, interdendritic melt in the columnar trunk, and solid dendrites in the columnar trunk. They are quantified by the volume fractions ( $f_\ell$, $f_{\mathrm{d}}^{\mathrm{e}}$, $f_{\mathrm{s}}^{\mathrm{e}}$, $f_{\mathrm{d}}^{\mathrm{c}}$, $f_{\mathrm{s}}^{\mathrm{c}}$), and characterized by different solute concentrations. The interdendritic melt and solid dendrites in the equiaxed grain combine to form a 'hydrodynamic' phase, i.e. e-phase, moving with an average velocity ($\vec{u}_{\mathrm{e}}$), while the interdendritic melt and solid dendrites in the columnar trunk combine to form another 'hydrodynamic' phase, i.e. c-phase, moving with a predefined velocity ($\vec{u}_{\mathrm{c}}$). The interdendritic melt is separated from the extra melt by a grain boundary (envelope). The volume fraction of each phase region inside the corresponding grain envelope is denoted as $\alpha_{\mathrm{d}}^{\mathrm{e}}$, $\alpha_{\mathrm{s}}^{\mathrm{e}}$, $\alpha_{\mathrm{d}}^{\mathrm{c}}$, $\alpha_{\mathrm{s}}^{\mathrm{c}}$. The extra melt is regarded as a third 'hydrodynamic' phase, i.e. $\ell$-phase, flowing with the velocity ($\vec{u}_\ell$). The velocity fields are solved on the 'hydrodynamic' phases. The transport of mass, species and energy of each phase region will be calculated based on the velocity of the corresponding 'hydrodynamic' phase. As shown in Fig. 1, the columnar tip front, which must be explicitly tracked, divides the whole calculation domain into two. In front of the columnar tip front, the maximum number of 'hydrodynamic' phases is 2, i.e. $\ell$-phase and e-phase, there only maximum 3 phase regions are involved. However, behind the columnar tip front, all the 3 'hydrodynamic' phases and all the 5 phase regions might be involved.

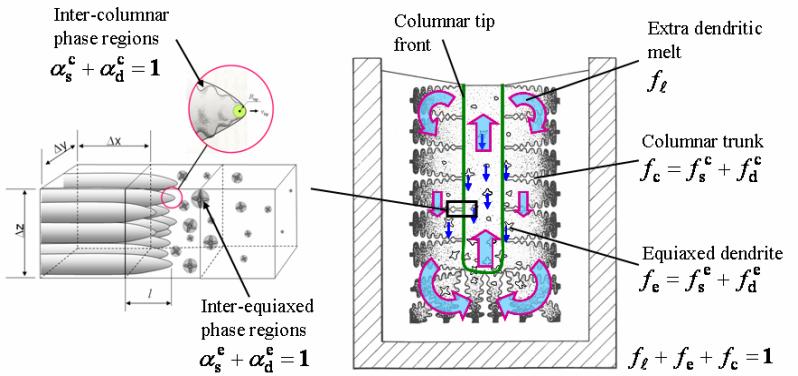


Figure 1. Schematic of the mixed columnar-equiaxed solidification.

*Equiaxed dendrite morphology*

An improved model for the equiaxed dendritic solidification was presented previously [7]. As shown in Fig. 2, the grain envelope (dash line) of the equiaxed grain is defined as a fictitious surface connecting the primary and secondary dendrite tips. The interdendritic melt has an average concentration $c_{\mathrm{d}}^{\mathrm{e}}$, while the extra melt has a concentration $c_\ell$. The species transfer due to the grain growth and due to the species diffusive flux across the envelope must be considered. According to [1], a continuity condition of the solute distribution at the grain envelope must apply, and the average concentration at the grain envelope $c_{\mathrm{env}}^{\mathrm{e}}$ is neither equal to $c_{\mathrm{d}}^{\mathrm{e}}$ nor to $c_\ell$. Solidification occurs at the liquid-solid interface, i.e. the interface between the interdendritic melt and solid dendrites. The interdendritic melt and solid adjacent to the liquid-solid interface has the thermodynamic equilibrium concentrations $c_\ell^*$ and $c_{\mathrm{s}}^*$. In the

interdendritic melt region, it is the concentration difference ($c_\ell^* - c_d^e$) that serves as driving force for the solidification of the interdendritic melt. Solute partitioning ($k = c_s^* / c_\ell^*$) occurs at the liquid-solid interface.

One drawback of the above envelope is that we can not determine the growth velocity along the envelope (dash line). What is known is the primary tip velocity $v_{tip'}^e$, which can be determined according to the Lipton-Glicksman-Kurz (LGK) model [8]. Therefore, the shape of the equiaxed dendritic grain is further simplified as an 'equivalent sphere', whose volume is equal to the volume enclosed in the grain envelope. The correlation between the growth velocity of the equivalent sphere and the primary tip is made by considering a shape factor $\Phi_{env,}^e$ [7]:

$$v_{env,M}^e = \Phi_{env}^e \cdot v_{tip'}^e \tag{1}$$

In order to calculate the species diffusive flux across the grain envelope from the interdendritic melt to the extra dendritic melt, however, the real surface area of the envelope $S_{env,D}^e$ is required. This area $S_{env,D}^e$ is actually correlated to the surface area of the equivalent sphere ($S_{env,M}^e$) by another factor $\Phi_{sph}^e$, here is called sphericity,

$$S_{env,D}^e = S_{env,M}^e / \Phi_{sph}^e \tag{2}$$

Both $\Phi_{env}^e$ and $\Phi_{sph}^e$ are two morphological parameters, dependent purely on the shape of the grain envelope. If the shape of the envelope is preserved, both parameters should be constant and can be determined previously. For example, in the Rappaz and Thevoz's model [3-4], where an ideal spherical envelope connecting the primary dendrite tips is assumed, both $\Phi_{env}^e$ and $\Phi_{sph}^e$ are equal to one. For an octahedral envelope connecting the primary dendrite tips as Nielsen et al. did [9], the $\Phi_{env}^e$ is $1/\sqrt[6]{\pi}$ and $\Phi_{sph}^e$ is $\sqrt[3]{\pi}/\sqrt{3}$. For a more realistic grain envelope (Fig. 2), both morphological parameters can be much smaller than the values of above.

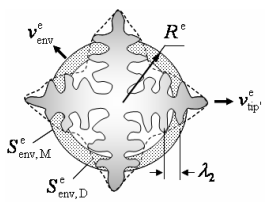


Figure 2: The shape of the equiaxed dendritic grain is simplified as a sphere with the equivalent volume of the grain envelope which connects the primary and secondary dendrite tips.

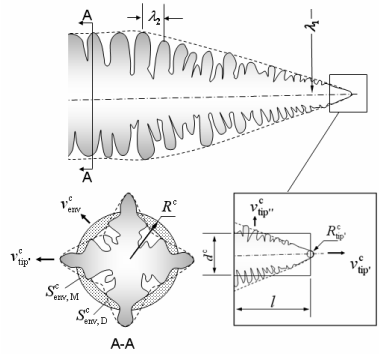


Figure 3: The shape of the columnar dendrite trunk is simplified as a step-wise cylinder with the cross section area equivalent to the tree-trunk envelope which connects the secondary and ternary dendrite tips. The parabolic shape of the columnar envelope near the primary dendrite tip is simplified as equivalent cylinder with an average diameter.

*Columnar dendrite morphology*

For the columnar growth, the dendrite trunk is assumed to be confined in a fictitious grain envelope, as shown in Fig. 3. Near the primary dendrite tip, it encloses the primary and secondary dendrite tips, while in the dendrite trunk region (away from the primary dendrite tip)

it encloses the secondary and ternary dendrite tips. The longitudinal section of the envelope near to the primary dendrite tip is parabolic, the cross section of dendrite trunk can be approximated by a quadrate or cloverleaf. Therefore, the model to treat the region near primary dendrite tip is different from the one to treat the columnar dendrite trunk region.

For the columnar dendrite trunk region, the grain envelope is further simplified as step-wise cylinder with the cross section area equivalent to the enclosed area of the grain envelope. The term 'step-wise' means that the dendrite trunks which are located in one volume element, simplified as a cylinders, have a constant averaged diameter, but they may have a different diameter in the neighbour volume element. The growth speed of the equivalent cylinder can be calculated from the growth velocity of the secondary dendrite tip $v^{c}_{tip''}$,

$$v^{c}_{env,M} = \Phi^{c}_{env} \cdot v^{c}_{tip''} \tag{3}$$

where $\Phi^{c}_{env}$ is a shape factor. The diffusion area of the columnar envelope ( $S^{c}_{env,D}$ ) is estimated based on the surface area of the equivalent cylinder ( $S^{c}_{env,M}$ ) by considering a circularity $\Phi^{c}_{circ}$,

$$S^{c}_{env,D} = S^{c}_{env,M} \big/ \Phi^{c}_{circ} \tag{4}$$

When the original envelope of dendrite trunk is described with an ideal cylinder, both $\Phi^{c}_{env}$ and $\Phi^{c}_{circ}$ are equal to one. If cross section of the dendrite trunk is approximated with a quadrate, the $\Phi^{c}_{env}$ is equal to $\sqrt{2/\pi}$ and $\Phi^{c}_{circ}$ is $\sqrt{\pi}/2$. For a more realistic tree trunk envelope, both morphological parameters are smaller than the values of above.
In the volume element, containing primary dendrite tips, the parabolic envelope of the primary dendrite tip region is approximated as an volume-equivalent cylinder with an averaged diameter $d^{c}$ and length $l$ (Fig. 3). The length of the cylinder is explicitly tracked with a method which is described in [10]. With the corresponding shape factor and circularity, the dendritic morphology of the primary dendrite tip region is modelled.

*Growth of equiaxed dendrites*

According to [7], two situations are distinguished: globular growth and dendritic growth. For the globular growth, solute partitioning occurs at the liquid-solid phase boundary (identical to the grain boundary). The growth of the grain is governed by diffusion, and its growth velocity $v^{e}_{glob}$ can be modeled analytically.

$$v^{e}_{glob} = \frac{D_{\ell}}{R^{e}} \cdot \Omega \tag{5}$$

$\Omega$ is the constitutional undercooling $\left(c^{*}_{\ell} - c_{\ell}\right) / \left(c^{*}_{\ell} - c^{*}_{s}\right)$. For the dendritic growth, the growth velocity of the dendrite tips can be determined by the LGK model [8].

$$v^{e}_{tip'} = \frac{D_{\ell} \cdot m_{\ell} \cdot c^{*}_{\ell} \cdot (k-1)}{\Gamma \cdot \pi^{2}} \left(\mathrm{Iv}^{-1}(\Omega)\right)^{2} \tag{6}$$

With Eq.(1) the growth velocity of the volume-equivalent sphere of dendritic grain $v^{e}_{env,M}$ is obtained. The globular to dendritic transition (GDT) is determined by comparing the two growth velocities. Therefore, the general formulation for the growth velocity of the equivalent spherical grain is:

$$v^{e}_{env} = \max\left(v^{e}_{glob},\ v^{e}_{env,M}\right) \tag{7}$$

The growth surface area concentration $S^{e}_{env,M}$ of the equivalent spheres is calculated

$$S^{e}_{env,M} = \Phi^{e}_{Imp} \cdot \left(36\pi \cdot n\right)^{\frac{1}{3}} \cdot f_{e}^{\frac{2}{3}} \tag{8}$$

where $n$ is number density of the grains, $\Phi^{e}_{Imp}$ is an impingement factor of the grains. With the above $v^{e}_{env}$ and $S^{e}_{env,M}$, the volume averaged mass transfer rate from $\ell$-phase to e-phase can be calculated.

*Growth of columnar dendrites*

Two situations are distinguished: cellular growth (no developed dendrites) and dendritic growth. For the cellular growth, its growth velocity $v^{c}_{cell}$ is governed by the diffusion,

$$v^{c}_{cell} = \frac{D_{\ell}}{R^{c}} \cdot \Omega \cdot \ln^{-1}\left(\frac{\lambda_1}{\sqrt{3}R^{c}}\right) \tag{9}$$

Here a stagger arrangement of the columnar trunks is assumed. The actual columnar diameter is $2R^{c}$, and the maximum diameter of the columnar is $2\lambda_1/\sqrt{3}$. For the dendritic growth, the growth velocity of the secondary dendrite tip is determined by the LGK model [8].

$$v^{c}_{tip''} = \frac{D_{\ell} \cdot m_{\ell} \cdot c^{*}_{\ell} \cdot (k-1)}{\Gamma \cdot \pi^{2}} \left(\mathrm{I}v^{-1}(\Omega)\right)^{2} \tag{10}$$

With Eq.(3) the growth velocity of the volume-equivalent cylinder $v^{c}_{env,M}$ is obtained. The cellular to dendritic transition (CDT) is determined by comparing the two growth velocities. Therefore, the general formulation for the growth velocity of the equivalent envelope is:

$$v^{c}_{env} = \max\left(v^{c}_{cell},\ v^{c}_{env,M}\right) \tag{11}$$

The growth surface area concentration $S^{c}_{env,M}$ of the equivalent cylinder is calculated

$$S^{c}_{env,M} = \Phi^{c}_{Imp} \cdot \frac{2\pi R^{c}}{\lambda_1^{2}} \tag{12}$$

where $\Phi^{c}_{Imp}$ is an impingement factor of the columnar trunks. With the above $v^{c}_{env}$ and $S^{c}_{env,M}$, the volume averaged mass transfer rate from $\ell$-phase to c-phase in the volume elements, which contain the fully through-grown columnar trunks, can be calculated.

In the volume elements, which contain columnar tips, some special considerations must be made. For the growth of the equivalent cylindrical envelope in the radius direction, the same idea of Eq.(9)-(11) is used to get $v^{c}_{env}$, but the length of the columnar trunks which belongs to the volume element and the diameter of them must be tracked explicitly [10]. Additionally, the contribution of the growth of the primary tips themselves ($v^{c}_{tip'} \cdot \pi R^{c}_{tip'}{}^{2}$) to the total volume averaged mass transfer in the considered volume element must also be taken into account. The tip radius $R^{c}_{tip'}$ is according to Kurz and Fisher [11], and the primary tip growth velocity $v^{c}_{tip'}$ is according to Kurz-Giovanola-Trivedi (KGT) model [12],

$$v^{c}_{tip'} = k_1 \cdot \Delta T^{2} + k_2 \cdot \Delta T^{3} \tag{13}$$

where $k_1$ and $k_2$ are empirical growth parameters, and $\Delta T$ is undercooling.

*Solidification of interdendritic melt*

The solidification of the interdendritic melt is treated in the same way for both equiaxed and columnar growth. Therefore, we take only equiaxed solidification as an example. The solidification rate of interdendritic melt is determined by the $\ell$/s interface growth velocity $v^{e}_{sd}$ and the $\ell$/s interface area concentration $S^{e}_{s}$. The driving force for $v^{e}_{sd}$ is $c^{*}_{\ell} - c^{e}_{d}$, but is governed by diffusion in the diffusion length scale $l^{e}_{d}$ relating to the secondary arm spacing $\lambda_2$ [1]:

$$l_{\mathrm{d}}^{\mathrm{e}} = \beta_2 \cdot \frac{(\lambda_2 - d_2)}{2} \qquad (14)$$

where $\beta_2$ is a constant in the order of unity, $d_2$ is the diameter of the secondary dendrite arms. We assume that $d_2$ is correlated to $\lambda_2$ by $\lambda_2 - d_2 = \lambda_2 \cdot \alpha_{\mathrm{d}}^{\mathrm{e}}$. So,

$$v_{\mathrm{sd}}^{\mathrm{e}} = \frac{2 \cdot D_\ell}{\beta_2 \cdot \lambda_2 \cdot \alpha_{\mathrm{d}}^{\mathrm{e}}} \cdot \frac{c_\ell^* - c_{\mathrm{d}}^{\mathrm{e}}}{c_\ell^* - c_{\mathrm{s}}^*}. \qquad (15)$$

The $\ell$/s interface area in an enclosed grain envelope is also related to the secondary arm spacing ($\propto 2/\lambda_2$) [1]. Considering an impingement factor $\Phi_{\mathrm{Imp}}^{\mathrm{s}}$ ($=\alpha_{\mathrm{d}}^{\mathrm{e}}$) of the growing surface areas, the $\ell$/s interface area concentration regarding to the total volume can be derived as

$$S_{\mathrm{s}}^{\mathrm{e}} = \frac{2 \cdot \Phi_{\mathrm{Imp}}^{\mathrm{s}}}{\lambda_2} \cdot f_{\mathrm{e}}. \qquad (16)$$

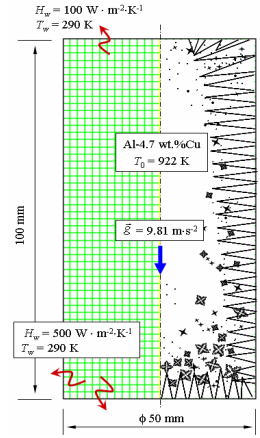


Figure 4: Schematic of the simulation benchmark (Al-4.7wt.%Cu) and boundary conditions.

## Modelling example

A 2D axis-symmetrical casting ($\phi$ 50x100 mm$^2$) with Al-4.7wt.%Cu binary alloy is simulated (Fig. 4). Mould filling is ignored. The casting starts to solidify from an initial temperature of 922 K. Both the mould temperature and the heat transfer coefficient at mould-casting interface are set constant. The thermo physical and dynamical data used are given elsewhere [7,14], and some other modelling parameters are listed in Table 1.

Table 1. Parameters used for the simulation

| | |
|---|---|
| Nucleation parameters:<br>$n_{\max} = 5 \times 10^{10}$ m$^{-3}$, $\Delta T_N = 10$ K<br>$\Delta T_\sigma = 0.5$ K | Morphological parameters:<br>$\Phi_{\mathrm{env}}^{\mathrm{e}} = 0.6827$; $\Phi_{\mathrm{sph}}^{\mathrm{e}} = 0.283$;<br>$\Phi_{\mathrm{env}}^{\mathrm{c}} = 0.7979$; $\Phi_{\mathrm{circ}}^{\mathrm{e}} = 0.295$;<br>$\lambda_1 = 500$ μm; $\lambda_2 = 10$ μm. |
| Growth kinetics parameters in KGT model[12,13]:<br>$k_1 = 1.16633 \times 10^{-4} \cdot (100 \cdot c_\ell)^{-1.24319}$<br>$k_2 = 5.39996 \times 10^{-4} \cdot (100 \cdot c_\ell)^{-2.13518}$ | |

The solidification sequence at 8.8 seconds is shown in Fig. 5. Equiaxed grains start to nucleate and grow from corner and surface regions, while columnar trunks grow directly from the mould walls. Both equiaxed grains and columnar trunks grow competitively. Large amount of equiaxed grains sink along the columnar tip front and settle in the bottom region. The equiaxed grains grow while sinking. The sinking grains drag the melt with them, inducing an axis-symmetrical circulation current. In the mean time the flow between the columnar dendrite trunks is slowed down by the mushy zone. The equiaxed grains, when they are entrapped between the columnar trunks, can not move any more. This entrapment phenomenon is more evidently observed in the bottom region when large amount of equiaxed grains settle there. Different mass transfer rates $M_{\ell \mathrm{c}}$, $M_{\mathrm{ds}}^{\mathrm{c}}$, $M_{\ell \mathrm{e}}$, $M_{\mathrm{ds}}^{\mathrm{e}}$, shown in Fig.5, give further indications about the competitions between the growth rate of the grain envelope and the solidification rate of interdendritic melt. When the grain growth rate is larger than the interdendritic melt

solidification rate, the grain becomes more dendritic. The results on the phase volume fraction inside the grain envelope( $\alpha_s^c, \alpha_d^c, \alpha_s^e, \alpha_d^e$ ) is also available, but not shown here due to the limited space.

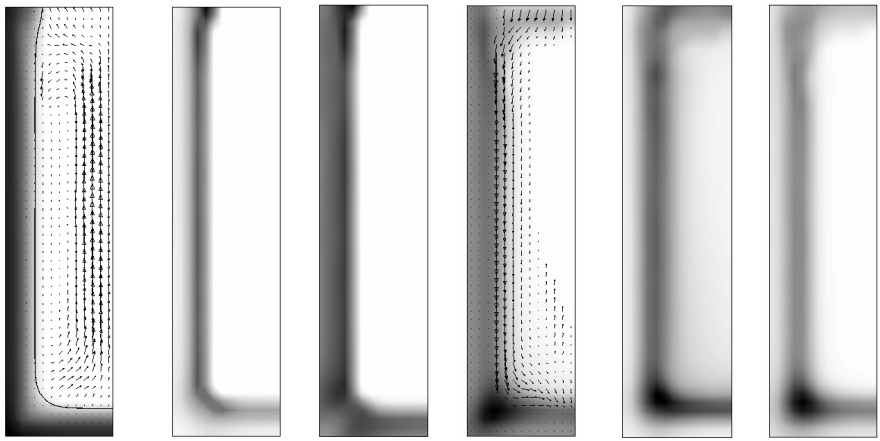

a) $f_c$ (-0.62), $\vec{u}_\ell$ (1.25 $\mathrm{mm \cdot s^{-1}}$) b) $M_{\ell c}$ (-194 $\mathrm{kg \cdot m^{-3} \cdot s^{-1}}$) c) $M_{ds}^c$ (-88 $\mathrm{kg \cdot m^{-3} \cdot s^{-1}}$) d) $f_e$ (-0.5), $\vec{u}_e$ (3.53 $\mathrm{mm \cdot s^{-1}}$) e) $M_{\ell e}$ (-191 $\mathrm{kg \cdot m^{-3} \cdot s^{-1}}$) f) $M_{ds}^e$ (-132 $\mathrm{kg \cdot m^{-3} \cdot s^{-1}}$)

Figure 5. Solidification sequence at 8.8 s. Only half section is shown. All the scalar quantities are grey scaled with dark for the highest and light for the lowest value. The velocity vectors are linearly scaled from 0 to the maximum. The volume fraction of the c-phase $f_c$ is overlain by the liquid velocity $\vec{u}_\ell$. Columnar tip position is plotted together with $f_c$. The mass transfer rate from $\ell$-phase to c-phase is quantified by $M_{\ell c}$. The solidification rate, which occurs inside the columnar trunks, is quantified by $M_{ds}^c$.The volume fraction of the e-phase $f_e$ is overlain by the equiaxed velocity $\vec{u}_e$. The mass transfer rate due to equiaxed growth is quantified by the $M_{\ell e}$. The solidification rate inside the equiaxed grains is quantified by $M_{ds}^e$.

The predicted final macrostructure is shown in Fig.6-7. Demonstratively, the most important structural information, such as the distinguished columnar and equiaxed zones ( $f_c$ and $f_e$) separated by the CET line, the average equiaxed grain size $d^e$ and diameter of the columnar trunks $d^c$, the eutectic phases formed in the interdendritic region $f_{Eu}^{intern}$ and extra grain(or extra columnar) region $f_{Eu}^{extra}$, and the final macrosegregation $c_{mix}$ pattern, can be obtained. This numerical prediction agrees to some extent with experimental results, often observed in aluminium ingots [15-16], but further model refinements and quantitative evaluations by comparison with experiments are still required.

## Summary

A new five-phase volume averaged solidification model is presented. The main features of the model are: mixed columnar-equiaxed solidification including columnar-to-equiaxed transition, morphological transition (globular-to-dendritic for equiaxed, and cellular-to-dendritic for columnar), melt convection and grain sedimentation, formation of eutectic phases including the extra grain (or extra columnar) eutectic and interdendritic eutectic, macrosegregation, etc. Preliminary modeling result on an Al-4.7wt.Cu casting has reproduced the macrostructure distribution pattern observed in some classical experiments, but further modeling refinements and quantitative evaluations and verifications are still required.

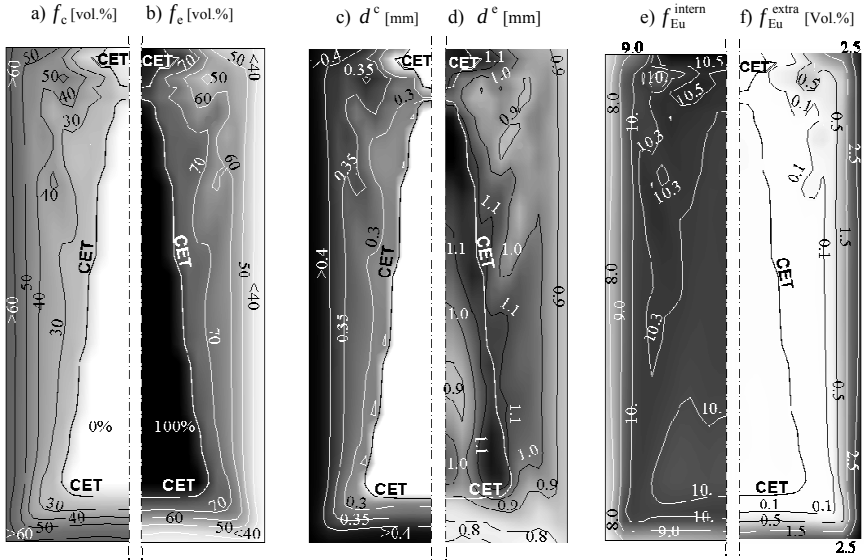


Figure 6. Predicted macrostructure. The quantities are shown in gray scale and isolines. The position of columnar-to-equiaxed transition is indicated with CET line. a) volume fraction of the columnar dendrite trunks; b) volume fraction of the equiaxed grains; c) averaged diameter of the columnar trunks; d) averaged diameter of the equiaxed grains; e) volume fraction of the interdendritic eutectic phase including those in equiaxed grains and in columnar trunks; f) volume fraction of the extra grain eutectic phase.

## References


1. C.Y. Wang and C. Beckermann, *Metall. Trans.*, 24A(1993), 2787-2802.
2. C.Y. Wang and C. Beckermann, *Metall. Mater. Trans.*, 27A(1996), 2754-64.
3. M.Rappaz and Ph.Thévoz, *Acta Metall.*, 35(1987), 1487-97.
4. M.Rappaz and Ph.Thévoz, *Acta Metall.*, 35(1987), 2929-33.
5. M.Wu and A. Ludwig, *Metall. Mater. Trans.*, 37A(2006), 1613-31.
6. A. Ludwig and M. Wu, *Mater. Sci. Eng. A*, 413-414(2005), 109-114.
7. M. Wu and A. Ludwig, *Proc. 5th Decennial Intern. Conf. Solidification Processing*, Ed. H. Jones., (Padstow: Tj Intern. Ltd., 2007), 130-134.
8. J.Lipton, M.E. Glicksman and W. Kurz, *Mater. Sci. Eng.*, 65(1984), 57-63.
9. Ø. Nielsen, B.Appolaire, H. Combeau and A. Mo, *Metall. Mater. Trans.*, 32A(2001), 2049-60.
10. M.Wu and A. Ludwig, *Metall. Mater. Trans.*, 38A(2007), 1465-75.
11. W. Kurz and D.J. Fisher, *Fundamentals of Solidification*, (Aedemannsdorf: Trans Tech Publications, 1989).
12. W.Kurz, B.Giovanola and R.Trivedi, *Acta Metall.*, 34(1986), 823-830.
13. S.Y.Lee, S.M.Lee and C.P.Hong, *ISIJ Int.*, 40(2000), 48-57.
14. M. Wu, A. Ludwig and J. Luo, *Mater. Sci. Forum*, 475-479(2005), 2725-2730.
15. R. Morando, H. Biloni, G.S. Cole, and G.F. Bolling, Metall. Trans., 1(1970), 1407-12.
16. A. Ohno, *Solidification – The separation theory and its practical applications*, (Berlin: Springer-Verlag, 1987), 1-123.


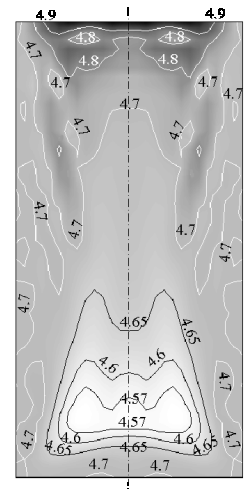

Figure 7. Final macrosegregation pattern, i.e. $c_{mix}$ [wt.%], shown in gray scale and isolines.